Zhang, Z., Yuan, X., Chen, Y., Tian, X., Kind, R., Li, X., Teng, J. (2010): Seismic signature of the collision between the east Tibetan escape flow and the Sichuan Basin. - Earth and Planetary Science Letters, 292, 3-4, 254-264

DOI: 10.1016/j.epsl.2010.01.046

Seismic signature of the collision between the east Tibetan escape flow and the Sichuan Basin

Zhongjie Zhang[1], Xiaohui Yuan[2], Yun Chen[1], Xiaobo Tian[1], Rainer Kind[2,3], Xueqing Li[2] & Jiwen Teng[1]

[1] State Key Laboratory of Lithosphere Evolution, Institute of Geology and Geophysics, Chinese Academy of Sciences, Beijing, 100029, China (zhangzj@mail.iggcas.ac.cn)

[2] Deutsches GeoForschungsZentrum GFZ, Telegrafenberg, 14473 Potsdam, Germany

[3] also at Freie Universität Berlin, Germany

Abstract

GPS displacement vectors show that the crust in east Tibet is being squeezed in an easterly direction by the northward motion of the Indian plate, and the Sichuan Basin is resisting this stream and redirecting it mainly towards Indochina. The Longmen Shan, containing the steepest rise to the high plateau anywhere in Tibet, results from the strong interaction between the east Tibetan escape flow and the rigid Yangtze block (Sichuan Basin), but the kinematics and dynamics of this interaction are still the subject of some debates. We herein present results from a dense passive-source seismic profile from the Sichuan Basin into eastern Tibet in order to study the deep structure of this collision zone. Using P and S receiver function images we observe a sudden rise of the Lithosphere-Asthenosphere Boundary (LAB) from 120-150 km beneath the Sichuan Basin to 70-80 km beneath eastern Tibet. In contrast, the depth of the crust-mantle boundary (Moho) increases from 36-40 km beneath the Sichuan

Basin to 55-60 km beneath eastern Tibet. The 410 km discontinuity is depressed below eastern Tibet by about 30 km, although the 660 remains at nearly the same depth throughout the LMS. From these observations, we conclude that the mode of collision that occurs between Tibet and the Sichuan Basin is very different to that found between India and Tibet. In southern Tibet, we observe in essence the subduction of the Indian plate, which penetrates northwards for several hundred kilometers under central Tibet. The very thin mantle part of the lithosphere beneath eastern Tibet may indicate delamination or removal of the bottom of the lithosphere by hot asthenospheric escape flow. This process leads to the exceptionally steep topography at the eastern Tibetan margin as a result of gravitational buoyancy. This view is supported by the very unusual depression of the 410 km discontinuity beneath eastern Tibet, which could be caused by the dynamics of the sub-vertical downward asthenospheric flow.

Keywords: East Tibetan escape flow, Sichuan Basin, receiver function imaging, mantle transition zone.

1. Introduction

As a result of the continuous convergence between the Indian and Eurasian tectonic plates that has been taking place over approximately the last 45 million years, it is estimated that the crust in the collision zone has been shortened by at least 1500 km (Molnar & Tapponnier, 1975; Armijo et al., 1986; England & Houseman, 1986; England & Molnar, 1997; Yin, 2000). Subsurface compensation may have occurred in a variety of different ways, such as by crustal

thickening (Allegrè, 1984), denudation (Meng et al., 2006), slip partitioning (Chen et al., 1994; Tapponnier et al., 2001), subduction of the Indian mantle lithosphere (Kosarev et al., 1999; Kumar et al., 2006; Li et al., 2008a), lithospheric detachment (Houseman et al., 1981, Molnar, 1988), subduction of the Asian lithosphere (Willett and Beaumont, 1994; Kind et al., 2002) and eastward escape (Royden et al., 1997, 2008; Clark and Royden, 2000; Klemperer, 2006). GPS displacement vectors (Gan et al., 2007) and SKS anisotropy measurements (Wang et al., 2008) indicate that the Tibetan crust (and possibly also the lithosphere and asthenosphere) is escaping eastwards, and that the main portion of the flow is being redirected towards the south east after it encounters the Sichuan Basin (Figure 1). As part of the Yangtze craton, the Sichuan Basin is an old, intact block that remained undeformed during the orogenic events that formed the Tibetan plateau. Anomalously cold temperatures derived from tomographic observations extend down to at least ca 200 km beneath the Sichuan Basin and are also present in the Mantle Transition Zone (MTZ) to the east and south-east of the Sichuan Basin (Li et al., 2008a, Yi et al 2008). However, the mode of collision that occurs between the Tibetan and Sichuan lithospheres (e.g. thickening or subduction) remains poorly understood. The powerful interaction between eastern Tibet and the Sichuan Basin is characterized by the Longmen Shan (LMS), which has the steepest topography gradient in Tibet (Royden et al., 1997; Clark and Royden, 2000; Klemperer, 2006). The LMS fault system, which marks the border of the Songpan-Ganzi block of eastern Tibet and the Sichuan block of the Yangtze craton, is dominated by dextral strike-slip and has a significant thrust component (Burchfiel et al., 1995**;** 2008). The 12 May 2008 Wenchuan earthquake, characterized by a crustal shortening of 8.5 m and an uplift of 7.5 m, confirms the view that

the east Tibetan escape flow is responsible for the high topography in this region (Xu et al. 2009).

In order to study the nature of the collision occurring between the Tibetan and the Sichuan lithospheres, we conducted a passive seismic experiment across the LMS fault belt at the eastern rim of the Tibetan plateau between August 2006 and July 2007. This data set has yielded images of crustal variations across the LMS fault belt that support lower crustal channel flow or tectonic escape (Zhang et al., 2009). The deeper structure of the same profile is analyzed herein. We use the teleseismic P and S receiver functions (Langston, 1977; Vinnik, 1977; Farra & Vinnik, 2000) to detect converted seismic waves from the crust-mantle boundary (Moho), from the Lithosphere-Asthenosphere Boundary (LAB), and from the discontinuities at 410 km and 660 km depth that confine the MTZ. This provides a good opportunity to understand the shallow and deep interactions that occur between the Tibetan escape flow and the resistive Sichuan Basin.

2. Data acquisition and generation of receiver function images

2.1 Moho and LAB from P and S receiver functions

We used a teleseismic data set consisting of one year of data obtained from 29 three-component seismic stations (nine Reftek-130 and twenty Reftek-72A data loggers and Guralp CMG 3ESP sensors) along the profile in the western part of Sichuan Province (Figure 1). In

these observations, stations S01-S07 were located in the Sichuan Basin and stations S13-S29 were located in the Songpan-Ganzi block, with station intervals of ~15 km. Stations S08-S12 were located in the LMS thrust fault zone at intervals of 10 km (Zhang et al., 2009). During the period of observation, we recorded 264 earthquakes of magnitude Ms > 5.0 in the distance range between 30 and 90 degrees (Figure 2a). We obtained 1823 Receiver Functions (RFs). The mean number of retained RFs per station was 64. Figure 2b shows all individual raw P receiver functions plotted in trace spacing within a time window of 0-80 s after P arrival for all 29 stations. The traces are moveout-corrected for a fixed ray parameter of 0.0573 s/km (corresponding to a slowness of 6.4 s/° or an epicentral distance of 67°) using the IASP91 reference model (Kennett & Engdahl, 1991). The figure serves to show the raw dataset. Piercing point locations of the mantle phases are not properly considered. No summation is applied to supress the noise level. To increase the coherence of the mantle phases a 5-s lowpass filter is applied to delay times later than 35 s. Signals from the Moho, LAB, 410 and 660 km discontinuities are marked. The Moho signal is red, which indicates that it is positive, and has a velocity that increases in the downward direction. A clear change in delay time of the Moho conversion is apparent between eastern Tibet and the Sichuan Basin. These times are about 6-8 s beneath the Songpan-Ganzi block (in eastern Tibet), and about 4-5 s beneath the Sichuan Basin. Details of the internal crustal structure derived from the same data set are given by Zhang et al. (2009) and may be summarized as follows: the Moho shallows from about 55-58 km under the Songpan-Ganzi block in eastern Tibet to 36-40 km under the western Sichuan Basin; a negative phase was observed in the lower crust under Songpan-Ganzi; the average crustal Vp/Vs ratios vary in the range 1.75-1.88 under Songpan-Ganzi in

east Tibet, and in the range 1.8-2.0 under the LMS fault belt, and decrease to less than 1.70 in the NW part of the Sichuan Basin. The results infered a low viscosity zone in the lower crust beneath eastern Tibet (Zhang et al. 2009). Figure 3 shows migrated P receiver functions down to a depth of 800 km. In Figure 2b, 410- and 660-km phases can be seen also though they are much weaker compared to Moho conversion phase and the signal/noise ratio is not very high. Then we convert these P receiver functions in time-domain into the migrated P receiver function image (Kind et al., 2002). The section was smoothed over 5 km in vertical direction and 60 km in horizonal direction,

The IASP91 model was used for migration. Figure 3 displays the resultant migrated P receiver function image. A clear blue signal (meaning negative amplitudes which indicate velocity decrease downward) is observed over the entire profile and interpreted as LAB. It is shallower beneath eastern Tibet than beneath the Sichuan Basin. This dip direction is opposite to that of the Moho. The LAB lies at a depth of about 70-80 km under east Tibet, at about 120 km under the western margin of the Sichuan Basin, and then deepens to about 150 km at the eastern end of our profile. The marked LAB in Figure 2b and Figure 3 might be argued as Moho phase sidelobe. A sidelobe has always more or less the same time difference to the main part of the signal, if the spacing between main part of the phase and the “sidelobe” varies from location to location then it can be considered as an independent phase mostly caused by the geological structure. The blue phase marked LAB in Figure 3 is indeed at the left side parallel and very close to the Moho which could give rise to the assumption that it is a sidelobe. However, if we look close to the LMS and the Sichuan Basin, LAB and Moho clearly separate which proofs that these two phases are independent. The Moho is shallowing and the LAB is deepening towards the right of the figure. In

order to check these results for the Moho and LAB structure, we applied S receiver function analysis, even though this data set is not as large as for the P receiver functions. The S receiver functions obtained along the profile are shown in Figure 4. Figure 4a shows the location of the boxes used for the summation of the traces. The LAB changes in depth below the LMS fault in an almost step-like fashion (Figures 3 and 4b) from about 70-80 km below eastern Tibet to 100-150 km below the Sichuan Basin, Similar depth of LAB beneath East Tibet is also reported by surface wave inversion (75-80 km, Lebedev and Agius, 2009). The shallower LAB beneath eastern Tibet than beneath the Sichuan Basin is confirmed by the S receiver function results (Figure 4b). Lower velocities at 100 km depth below eastern Tibet than below the Sichuan Basin as a consequence of the location of the LAB are supported by ambient noise surface wave tomography studies (Li et al., 2009) and other Rayleigh wave tomography studies (Li et al., 2008a; Yao et al., 2008; Yi et al., 2008).

2.2 410 km and 660 km discontinuities obtained from the P-receiver functions

The discontinuities at 410 km and 660 km are also clearly visible in the migrated section shown in Figure 3. Throughout the entire profile, the 660 is about 10-20 km below its global average value in the IASP91 model with only insignificant deepening below eastern Tibet. The 410, however, is exactly at the IASP91 value below the Sichuan Basin and clearly deepens towards eastern Tibet by about 30 km. In order to confirm this observation, we show in the time domain (Figure 5) the stacks of the P receiver functions. The binning stacks were obtained using a 150 km window of piercing points at a depth of 530 km. The window was

moved using a step length of 50 km.

Our receiver function signals from the 410 km discontinuity indicate that the clear change in lithospheric structure that occurs between eastern Tibet and the Sichuan Basin is also visible at the MTZ (Figure 3). The 410 is clearly deeper below eastern Tibet than below the Sichuan Basin. The 660 remains more stable. This results in a thinner MTZ below eastern Tibet than below the Sichuan Basin. No significant variation in MTZ thickness has been observed in central Tibet (Kind et al., 2002). In western Tibet, the MTZ has a uniform thickness between the Tarim Basin and the Kunlun range (Wittlinger et al., 2004). This could imply that any tectonic activity in central and western Tibet is confined to the upper mantle and does not reach down as far as 410 km below the surface. Contrary to that, the MTZ below the eastern margin of Tibet could be influenced by the lithospheric collision above.

The 410 km and 660 km discontinuities are commonly considered as mineral phase transformations of olivine into its high pressure forms, which cause sharp vertical gradients in density and seismic velocity. The 410 km discontinuity marks the transition from olivine to wadsleyite, and the 660 km discontinuity marks the transition from ringwoodite to perovskite + magnesiowustite. Experimental studies have shown that both reactions are sensitive to temperature and have Clapeyron slopes that are opposite in sign (Bina & Helffrich, 1994). In the absence of other effects, a lateral increase in temperature at the level of the transition zone should be reflected in a deepening of the 410 km discontinuity and a shallowing of the 660 km discontinuity (and vice versa). The temperature in the MTZ, which strongly influences the

mechanical strength of the mantle materials, can be derived from the thickness of the transition zone (Helffrich, 2000). Compared to the global average MTZ thickness of 250 km in the IASP91 global reference model (Kennett & Engdahl, 1991), the MTZ throughout our profile experiences a significant thinning of about 15 km to a thickness of 235 km beneath eastern Tibet. Beneath the western Yangtze block under the Sichuan Basin, however, it experiences a thickening of about 15 km to 265 km. This effect would lead to temperatures being raised in the MTZ under eastern Tibet by about 300 degrees compared to the Sichuan Basin. Tomographic velocity measurements (Li et al., 2008a; Yao et al., 2008), however, show higher velocities (meaning colder temperature and larger MTZ thickness) beneath eastern Tibet than below the Sichuan Basin, which contradicts the hypothesis that our observed thinning of the MTZ below eastern Tibet could be caused by increased temperature. We will return to a discussion of the variation in the thickness of the MTZ in Section 4.

3. Validation assessment of the Moho, LAB, 410 km and 660 km discontinuities

The identification of the Moho and the 410 km and 660 km discontinuities is a routine procedure in the analysis of P receiver functions. Our observations of these discontinuities are clear. However, we have also made observations of the LAB using the P receiver functions (Figures 2 and 3). The use of P receiver functions to study the LAB is generally characterized by problems caused by crustal multiples, because their presence often masks the LAB. No clear multiples are visible in our data, either in the time domain section (Figure 2b) or in the migrated section (Figure 3). In our case, the LAB cannot be mistaken for crustal multiples

because the signals associated with these should arrive much later beneath the thick eastern Tibetan crust than beneath the thinner crust of the Sichuan Basin. The phase marked LAB in Figure 3 shows the opposite trend. The P multiples within the crust below the Sichuan Basin must arrive after about 20 s, because the direct conversion arrives after about 5 s (see e.g. Yuan et al. 2002). This is much later than the arrival time of the LAB beneath the Sichuan Basin of about 12 s. Multiples do not show up in the S receiver functions in Figure 4b but the LAB is visible there. The LAB in Figures 3 and 4b can also not be caused by side lobes of the Moho signal because it appears at about the same depth in the longer period S receiver functions in Figure 4b and in the shorter period P receiver functions in Figure 3. Sidelobes would also be expected at a constant delay from the main signal which is clearly not the case in both P and S receiver functions. Observations of the LAB in P receiver functions are not unusual. Such observations have also been obtained worldwide by Rychert and Shearer (2009). S receiver functions are very useful for the verification of LAB observations, because of the absence of multiples (see e.g. Kumar et al. 2007). They are less commonly applied for this purpose, however, because there are usually fewer high quality S wave data available, especially in short term projects. The Moho and the LAB are visible in the S receiver functions in Figure 4, and arrive at approximately at the same time as in the P receiver functions (Figure 4b), although the piercing points of the P and S receiver functions are not identical. This confirms the observations of the Moho and LAB obtained from the P receiver functions. In order to confirm the P receiver function results from the MTZ in Figure 3, we have split the distribution of the piercing points into two regions (see Figure 6a) and computed two migrated profiles (Figure 6b). The essential features of the structure of the 410

km and 660 km discontinuities are preserved especially in the section A-A' in the northeast part of the region. The depth variation of the 410 km discontinuity is somewhat less pronounced along profile B-B' which could indicate a lateral variation of the 410 topography. These features are (1) the deepening of the 410 below eastern Tibet, (2) the agreement of the 410 below the Sichuan Basin with the IASP91 value and (3) the generally deeper 660 throughout the entire profile. Due to a lack of data, we could not obtain S receiver function data from the upper mantle.

The determination of the depth using measured differential times requires the use of a velocity model. Velocity models are not easily obtained from receiver function data. Techniques exist for inverting receiver function waveforms into velocity-depth models (e.g. Kind et al. 1995). However, such techniques are non-unique and we prefer not to use them here. Certain information may be obtained from receiver function images even if the velocity model is incomplete, i.e. the differential depths of the two discontinuities. For example, we may obtain the apparent thickness of the MTZ in Figure 3. The thickness of the MTZ depends only on the velocity within the transition zone and not on the velocity model above 410 km depth. This in turn means that the apparent thinning of the MTZ below eastern Tibet does not depend on the shallower structure. Li et al. (2008a) show high resolution tomographic velocity variations in the region of our profile. Their results indicate a velocity 2-3% higher at 400 km depth below eastern Tibet than below the Sichuan Basin. We observe a thinning of the transition zone of about 30 km, i.e. more than 10%, which means the thinning of the transition zone below eastern Tibet is indeed real and cannot be explained by a lateral velocity increase. It follows

from the same argument that the mantle part of the lithosphere (i.e. that is the difference between the LAB and the Moho) is independent of the crustal structure above it. Velocity measurements from around the Sichuan Basin were obtained by Yao et al. (2008), Li et al. (2008a) and Wang et al. (2007) from tomography and controlled source studies. According to Li et al. (2008a) the upper mantle shows almost 4% higher velocities down to at least 200 km depth beneath the Sichuan Basin than beneath eastern Tibet. From this we conclude that the observed time differences between the Moho and the LAB along our profile are caused by changes in the thickness of the mantle lithosphere and not changes in velocity. Otherwise, we would expect to see reversed time differences. Moho depths obtained from surface wave tomography in the south of our profile resulted in about 60 km depth beneath eastern Tibet and in about 40 km below the Sichuan Basin (Yao et al. 2008). Almost identical results for the Moho depths were obtained by Wang et al. (2007) from controlled source experiments. Topographic elevations and sedimentary coverage in the Sichuan Basin were considered in the results by Wang et al. (2007). Xu et al. (2007) also obtained very similar results for the Moho depths beneath the Sichuan Basin and eastern Tibet, using receiver function inversion from data obtained to the south of our profile. We used the IASP91 reference model to achieve the migration of our data and arrived at practically the same Moho depths. This shows that the migration of receiver functions is not very sensitive to the model changes. The reason for this is that in receiver function techniques, the P and S differential times are used and not absolute travel times. Differential times are more sensitive to the Vp/Vs ratio than to the absolute velocities.

4. Discussion of the variation in MTZ thickness across the Longmen Shan fault belt

4.1 MTZ thickening below Sichuan Basin from lower angle Pacific plate subduction?

The reason for the thickened MTZ below the Sichuan Basin relative to the global average is unclear. Changes in the thickness of the transition zone over such short distances have so far only been observed in subduction zones (Li et al., 2000; Liu et al., 2003; Li & Yuan, 2003; Tonegawa et al., 2006). In the following, we will discuss the possibility of the influence of lower-angle Pacific plate subduction on MTZ thickening beneath the Sichuan Basin. There are indications from tomography studies (e.g. Fukao et al. 2009) that a flat subduction of the Pacific plate in the MTZ in the north of the Yangtze Craton could reach as far as the Sichuan Basin (Lebedev et al., 2003; Li et al., 2008b). We have looked at P-to-S conversions from the 410 km and 660 km discontinuities at a number of seismic stations in China (see locations in Figure 7a) and found no indication of a large regional thickening of the MTZ that could be related to a flat Pacific slab inside the MTZ. The waveform data from these stations are shown in Figure 7b. Figure 7b indicates the observed differential times of the 410 km and 660 km discontinuities at an epicentral distance of 67°. The IASP91 value is 24 s. No significant contiguous zone of a thickened MTZ exists in relation to the slab stagnation of the western Pacific subduction zone. The maximum deviation from the 24 s global average value (marked by the blue line in Figure 7b) is ±2 s, corresponding to a variation in MTZ thickness of about ±10%.

4.2 Deepening of the 410 discontinuity below eastern Tibet

The deepening of the 410 discontinuity under eastern Tibet could possibly be caused by other factors than increased temperature. We hypothesize that the escape flow beneath eastern Tibet may also be turning downwards and subsiding into the MTZ, besides of its horizontal component in southeast direction. The thin mantle lithosphere below eastern Tibet would appear to support this view. The downwelling flow does not cause any increase in transition zone temperature, although it may be responsible for compositional differences in the MTZ, e.g. water content. Petrological studies have shown that the MTZ contains much more water than the mantle above and below it, because its main components (wadsleyite and ringwoodite) are known to be water-soluble (Bercovici & Karato, 2003; Ohtani et al., 2004). The dry and depleted asthenospheric material that sinks into the MTZ may reduce the water content of the MTZ. Laboratory experiments have shown that a decrease in water content in olivine may lower and broaden the 410 km discontinuity but increase the velocity jump across it, and vice versa (Yusa & Inoue, 1997; Chen et al., 2002). It therefore follows that a lateral variation in water content may change the topography of the 410 km discontinuity. Our observed thinning of the MTZ by around 15 km may conveniently be related to a reduction in water content within a downward asthenospheric escape flow. Additionally, in this particularly region the asthenospheric downwelling in front of the Sichuan block may be flowing fast enough to cause a dynamic deepening of the 410 km discontinuity as well, as proposed by Kirby et al. (1996) for subduction zones. We propose that both water-induced and dynamic depression of the olivine-wadsleyite transition may exist beneath eastern Tibet, thus accounting for the deepening of the 410 km discontinuity.

5. Sichuan Basin barrier to the eastward escape flow of eastern Tibet?

Our receiver function images show from the Sichuan Basin to eastern Tibet a steplike increase of about 20 km in the Moho depth, a decrease of about 50 km in the LAB depth and a decrease of about 30 km in the depth of the 410 discontinuity. Table 1 summarizes the depths of the LAB, and the 410 km and 660 km discontinuities beneath the stations along the profile. The crustal thickness beneath all 29 stations may be seen in Zhang et al. (2009). The previously mentioned systematic variations of crustal thickness, LAB and 410 beneath the LMS fault belt probably indicate that the Sichuan Basin acts as a barrier to the eastward escape flow of East Tibet that may extend to the whole lithosphere, even to the whole upper mantle.

The steepest topography gradient around the Tibetan plateau margin is commonly accepted to result from the strong interaction between the eastern Tibetan escape flow with the resistive Sichuan Basin. From our passive source seismic experiment, we contend that the deep process (or processes) that have occurred (and/or are occurring) beneath eastern Tibet may also contribute to the steep rise in topography at LMS, in addition to middle/lower crust channel flow and tectonic escape (Royden, 1996; Klemperer, 2006; Zhang et al., 2009). The convergence of the eastward escape flow from eastern Tibet with the Sichuan Basin should produce a downward undulation (or detachment according to Houseman et al. 1981) of the lithosphere beneath both the western margin of the Sichuan Basin and the eastern margin of eastern Tibet (Zhang et al., 2009). Our observation of a lithosphere just 70-80 km thick under

Songpan-Ganzi (east Tibet) probably results from delamination of a part of the lithosphere, as suggested by Houseman et al. (1981) and Houseman (1996), or from thermal erosion of the bottom of the lithosphere by the hot, eastward flowing, upper mantle (asthenosphere) beneath Tibetan plateau, or from both of these. This obvious lateral transition between eastern Tibet and the Sichuan Basin down to a depth of 400 km leads us to propose a two-phase accommodation of the shortening. The eastward flow of central and eastern Tibet meets the rigid barrier of the Sichuan Basin, which belongs to the western Yangtze block, and escapes partly into south eastern Tibet or north eastern Tibet around the Sichuan Basin, and is partly downwelling deep into the mantle. The lower part of the hot Tibetan lithosphere may be being delaminated due to collision with the colder Sichuan Basin, or alternatively the bottom of the lithosphere may be being removed by the hot asthenospheric escape flow. This idea could also explain the unusually thin mantle lithosphere beneath eastern Tibet. The delaminated material may be depressing the 410 km discontinuity dynamically. The asthenospheric vertical downward flow beneath the LMS fault belt due to the resistance of the Sichuan basin may be considered as an alternative way to compensate for the continuous convergence between the Indian and Eurasian plates. The extreme topographic relief across the LMS fault belt may be caused not only by lower crust channel flow in eastern Tibet (e.g. Royden et al., 1997, 2008; Clark and Royden, 2000; Klemperer, 2006; Zhang et al. 2009), but also by gravitational buoyancy due to lithospheric delamination (Houseman and England, 1986) or lithospheric bottom removal caused by hot asthenospheric escape flow. The residual (beneath the LAB) of the lithospheric delamination cannot confidentially be recognized in our data. Future studies are needed, such as high resolution seismic tomography or gravity modelling.

6. Conclusions

At the India-Tibet boundary, GPS displacements indicate a continuous northward flow of the Indian lithosphere of about 10mm/year (Gan et al. 2007). The resultant crustal shortening is accommodated by the subduction of the Indian lithosphere below the Tibetan lithosphere, as shown by numerous studies using receiver functions and tomographic methods (Kind et al., 2002, Wittlinger et al., 2004, Kumar et al., 2006, Li et al., 2008a). The Indian crust is probably separating from the mantle lithosphere and propagating as far as central Tibet at a shallow angle (Yuan et al. 1997, Kind et al. 2002, Li et al., 2008a; Royden et al., 2008; Nabelek et al. 2009; Zhang and Klempere, 2010), whereas the mantle lithosphere itself seems to be subducting deeper into the mantle. The depths of the upper mantle discontinuities directly below the collision zone are generally close to their global average values, indicating weak influence of the collision on the deeper part of the upper mantle. Recent receiver function observations in the eastern Himalaya show some modifications to the thickness of the MTZ that could be related directly to the collision (Singh and Kumar 2009). The processes occurring at the boundary between eastern Tibet and the Sichuan Basin seem to differ in a number of ways. GPS observations indicate that the Sichuan Basin is relatively immobile and that Tibet is moving in an easterly direction. GPS vectors obtained prior to the Wenchuan earthquake also show a redirection of the Tibetan flow around the Sichuan Basin and virtually no displacement near the boundary of the Sichuan Basin. Several meters of east-west shortening and uplift to the east of LMS caused by the Wenchuan earthquake have accommodated several thousand years of continuous displacement of Tibet in an easterly

direction. The crustal shortening of 8.5 m and an uplift of 7.5 m during the 12 May 2008 Wenchuan earthquake could not be well modeled with crustal deformation mechanism from only middle/lower crustal escape, and suggests that vertical force contribution to crustal deformation beneath Longmenshan and East Tibet could not be excluded (Zhang et al., 2008). The Moho under the NW Sichuan Basin is deepening towards Tibet to accommodate collisional shortening (Zhang et al., 2009), similar to the deepening of the Indian crust in a northerly direction. However, the LAB behaves in an opposite sense below the boundaries of Tibet in the south and east. In the south it is also subducting, along with the Moho, while at the border of eastern Tibet it is shallowing towards Tibet. The 410 km discontinuity is deepening directly underneath the deepening Moho in eastern Tibet. These two observations lead us to suggest the occurrence of delamination of the lower lithosphere below eastern Tibet, which reaches the 410 km discontinuity and is contributing to the rise of the eastern Tibetan margin by gravitational buoyancy (in addition to a lower crustal channel flow), which is similar to the suggestion made by Houseman (1996). Alternatively, the asthenospheric vertical downward flow beneath the LMS fault belt could be accelerating due to the rigid resistance of Sichuan Basin, as a means of compensating for the continuous convergence between the Indian and Eurasian plates.

Acknowledgements

We acknowledge the financial support of the Chinese Academy of Sciences (KZCX2-YW-132), the National Nature Science Foundation of China (#40721003 and #40830315), and the

Deutsche Forschungsgemeinschaft. XL thanks the Graduate University of Chinese Academy of Sciences and the Chinese Earthquake Network Center. We also thank Rixiang Zhu, Z. Bai, T. Xu and Zhi Zhang for their efforts in seismic data acquisition and for their constructive discussions with us. We would also like to thank Stephan Sobolev for his helpful comments. We acknowledge the suggestions made by Rob van de Hilst and two anonymous reviewers.

References

Allegrè, C. J. et al.,1984. Structure and evolution of the Himalaya–Tibet orogenic belt. *Nature* 307, 17– 22.

Armijo, R., Tapponnier, P., Mercier, J. L. & Han, T. L.,1986. Quaternary extension in southern Tibet: field observations and tectonic implications. *J. Geophys. Res.* 91, 13803–13872.

Bercovici, D. & Karato, S., 2003. Whole-mantle convection and the transition-zone water filter. *Nature* 425, 39-44.

Bina, C. R. & Helffrich, G.,1994. Phase transition Clapeyron slopes and transition zone seismic discontinuity topography. *J. Geophys. Res.* 99, 15853-15860.

Burchfiel, B. C., Chen, Z., Liu, Y. & Royden, L. H., 1995. Tectonics of the Longmenshan and adjacent regions. *Int. Geol. Rev*, 37, 661-735.

Burchfiel, B. C., Royden, L. H., van der Hilst, R. D. et al., 2008. A geological and geophysical context for the Wenchuan earthquake of 12 May 2008, Sichuan, People's

Republic of China. *GSA Today*, 18(7), doi:10.1130/GSATG18A.1.

Chen, J., T. Inoue, H., Yurimoto, D. & Weidner, J., 2002. Effect of water on olivine-wadsleyite phase boundary in the (Mg, Fe)$_2$SiO$_4$ system. *Geophys. Res. Lett.* 29, 1875, doi:10.1029/2001GL014429.

Chen, S. F., Wilson, C. J. L., Deng, Q. D., Zhao, X. L. & Luo, Z. L., 1994. Active faulting and block movement associated with large earthquakes in the Min Shan and Longmen mountains, northeastern Tibetan Plateau. *J. Geophys. Res.* 99, 24, 025–24,038.

Clark, M. K. & Royden, L. H., 2000. Topographic ooze: building the eastern margin of Tibet by lower crustal flow. *Geology* 28, 703-706.

England, P. & Houseman, G., 1986. Finite strain calculations of continental deformation: 2. Comparison with the India –Asia collision zone. *J. Geophys. Res.* 91, 3664–3676.

England, P. & Molnar, P., 1997. Active deformation of Asia: from kinematics to dynamics. *Science* 278, 647– 650.

Farra, V. & Vinnik, L., 2000. Upper mantle stratification by P and S receiver functions. G*eophys. J. Int.* 141, 699-712.

Fukao, Y., Obayashi, M. & Nakakuki, T., 2009. Stagnant slab: A review. *Annual Review of Earth and Planetary Sciences* 37, 19-46, DOI: 10.1146/annurev.earth.36.031207.124224

Gan, W., Zhang, P., Shen, Z., Niu, Z., Wang, M., Wan, Y., Zhou D. & Cheng, J., 2007. Present-day crustal motion within the Tibetan Plateau inferred from GPS measurements. *J. Geophys. Res.* 112, B08416, doi:10.1029/2005JB004120.

Helffrich, G., 2000. Topography of the transition zone seismic discontinuity. *Rev. Geophys* 38, 141-158.

Houseman, G.A., McKenzie, D.P. and Molnar, P., 1981. Convective instability of convective boundary-layer and its relevance for the thermal evolution of continental convergent belts. *J. Geophys. Res.* 86, 6115-6132.

Houseman, G. & England, P., 1986. A dynamic model of lithosphere extension and sedimentary basin formation. *J. Geophys. Res.*, 91,719-729.

Houseman, G., 1996. From mountains to basin. *Nature* 379, 771-772.

Huang, Z., Su, W., Peng, Y., Zheng, Y. & Li, H., 2003. Rayleigh wave tomography of China and adjacent regions. *J. Geophy. Res.* 108, 2073, doi:10.1029/2001JB001696.

Kennett, B. L. N. & Engdahl, R., 1991. Traveltimes for global earthquake location and phase identification. *Geophys. J. Int.* 105, 429-465.

Kind, R., Kosarev, G. L. & Petersen, N. V., 1995. Receiver functions at the stations of the German Regional Seismic Network (GRSN). *Geophys. J. Int*. 121, 191-202.

Kind, R., Yuan, X., Saul, J., Nelson, D., Sobolev, S.V., Mechie, J. Zhao, W., Kosarev, G., Ni, J., Achauer, U. & Jiang, M., 2002. Seismic images of crust and upper mantle beneath Tibet: evidence for Eurasian plate subduction. *Science* 298, 1219-1221.

Kirby, S. H., Stein, S., Okal, E. A. & Rubie, D. C., 1996. Metastable mantle phase transformations and deep earthquakes in subducting oceanic lithosphere. *Rev. Geophys.* 34, 261-306.

Klemperer, S. L., 2006. Crustal flow in Tibet: A review of geophysical evidence for the physical state of Tibetan lithosphere. In *Channel Flow, Ductile Extrusion and Exhumation of Lower Mid-Crust in Continental Collision Zones*, edited by M. P. Searle and R. D. Law, *Geol. Soc. Spec. Publ*., 268, 39-70.

Kosarev, G., Kind, R., Sobolev, S.V., Yuan, X., Hanka, W. & Oreshin, S., 1999. Seismic evidence for a detached Indian lithospheric mantle beneath Tibet. Science 283, 1306-1309.

Kumar, P., Yuan, X., Kind, R. & Ni, J., 2006. Imaging the colliding Indian and Asian lithospheric plates beneath Tibet. *J. Geophys. Res.*111, doi: 10.1029/2005JB003930.

Kumar, P., Yuan, X. H., Kumar, M. R., Kind, R., Li, X. Q. & Chadha, R. K., 2007. The rapid drift of the Indian tectonic plate. *Nature* 449, 894-897, DOI: 10.1038/nature06214.

Langston, C. A., 1977. Corvallis, Oregon, Crustal and upper mantle structure from teleseismic P and S waves. *Bull. Seism. Soc. Am*. 67, 713-724.

Lebedev, S. & Nolet, G., 2003. Upper mantle beneath southeast Asia from S velocity tomography. *J. Geophys. Res.* 108, doi:10.1029/2000JB000073.

Lebedev, S. Agius M., 2009. Seismic structure of Tibet: New constraints from surface wave. *Abstracts of 5th International Symposium on the Tibetan Plateau and 24th Himalaya-Karakorum-Tibet Workshop*, Beijing, China, S-1.13, pp30.

Li, C., van der Hilst, R., Meltzer, A. S. & Engdahl, E. R., 2008a. Subduction of the Indian lithosphere beneath the Tibetan Plateau and Burma. *Earth Planet. Sci. Lett* 274, 157-168.

Li, C., van der Hilst, R., Engdahl, E. R. & Burdick, S., 2008b. A new global model for P wave speed variations in Earth's mantle. *G*^{3} 9, Q05018, doi:10.1029/2007GC001806.

Li, H., W. Su, W., Wang, C.-Y. & Huang, Z., 2009, Ambient noise Rayleigh wave tomography in western Sichuan and eastern Tibet, *Earth and Planetary Science Letters*, 282, 201-211.

Liu, K. H., Gao, S., Silver, P. G. & Zhang, Y., 2003. Mantle layering across central South American. *J. Geophys. Res*. 108, 2510, doi:10.1029/2002JB002208.

Li, X., Sobolev, S. V., Kind, R., Yuan, X. & Estabrook, C., 2000. A detailed receiver function image of the upper mantle discontinuities in the Japan subduction Zone. *Earth Planet. Sci. Lett.* 183: 527-541.

Li, X. & Yuan, X., 2003. Receiver functions in northeast China - implications for slab penetration into the lower mantle in northwest Pacific subduction zone. *Earth Planet. Sci. Lett.* 216, 679–691.

Meng, Q., Hu, J., Wang, E. & Qu, H., 2006. Late Cenozoic denudation by large-magnitude landslides in the eastern edge of Tibetan Plateau. *Earth Planet. Sci. Lett.* 243, 252–267.

Molnar, P. & Tapponnier, P., 1975. Cenozoic tectonics of Asia: effects of a continental collision. *Science* 189, 419-426.

Molnar, P., 1988. Continental tectonics in the aftermath of plate tectonics. Nature 335, 131-137.

Nabelek, J., Hetenyi, G., Vergne, J., Sapkota, S., Kafle, B., Jiang, M., Su, H.P., Chen, J., Huang, B.S. & Hi-CLIMB Team. 2009. Underplating in the Himalaya-Tibet Collision Zone Revealed by the Hi-CLIMB Experiment. Science 325, 1371-1374, DOI: 10.1126/science.1167719.

Ohtani, E., Litasov, K., Hosoya, T., Kubo, T. & Kondo, T., 2004. Water transport into the deep mantle and formation of a hydrous transition zone. *Phys. Earth Planet. Int.* 143, 255–269.

Royden, L. H., Burchfiel, B. C., King, R. W., Wang, E., Chen, Z., Shen, F. & Liu, Y., 1997. Surface deformation and lower crustal flow in eastern Tibet. *Science* 276, 788–790.

Royden, L. H., Burchfiel, B. C. & van der Hilst, R. D., 2008. The geological evolution of the Tibetan plateau. *Science* 321, 1054-1058.

Rychert, C. A. & Shearer, P. M., 2009. A Global View of the Lithosphere-Asthenosphere Boundary. *Science* 324, 495-498, doi: 10.1126/science.1169754.

Singh, A. & Kumar, M. R., 2009. Seismic signatures of detached lithospheric fragments in the mantle beneath eastern Himalaya and southern Tibet. *Earth Planet. Sci. Lett.,* in press.

Tapponnier, P. et al., 2001. Oblique stepwise rise and growth of the Tibet Plateau. *Science* 294, 1671-1677.

Tonegawa, T., Hirahara, K., Shibutani, T. & Shiomi, K., 2006. Upper mantle imaging beneath the Japan Islands by Hi-net tiltmeter recordings. *Earth Planets Space* 58, 1007–1012.

Vinnik, L. P., 1977. Detection of waves converted from P to SV in the mantle. *Phys. Earth Planet. Int.* 15, 39-45.

Wang, C.-Y., Han, W.-B., Wu, J.-P., Lou, H. & Chan, W. W., 2007, Crustal structure beneath the eastern margin of the Tibetan Plateau and its tectonic implications, *J. Geophys. Res.*, 112, B07307, doi:10.1029/2005JB003873.

Wang, C. Y., Flesch, L. M., Silver, P. G., Chang, L. J. & Chan, W. W., 2008. Evidence for mechanically coupled lithosphere in central Asia and resulting implications. *Geology* 36, 363-366.

Willett, S.D. & Beaumont, Ch., 1994. Subduction of Asian Lithospheric mantle beneath Tibet inferred from models of continental collision. Nature 369, 642-645.

Wittlinger, G., Vergne, G., J., Tapponnier, P., Farra, V., Poupinet, G., Jiang, M., Su, H., Herquel, G. & Paul, A., 2004. Teleseismic imaging of subducting lithosphere and Moho offsets beneath western Tibet. *Earth Planet. Sci. Lett.* 221, 117–130.

Xu, L., Rondenay, S. & van der Hilst, R. D., 2007. Structure of the crust beneath the southeastern Tibetan Plateau from teleseismic receiver functions. *Phys. Earth Planet. Int.* 165, 176-193.

Xu, X., Wen, X., Yu, G., Chen, G., Klinger, Y., Hubbard, J. & Shaw, J., 2009. Coseismic reverse- and oblique-slip surface faulting generated by the 2008 Mw 7.9 Wenchuan earthquake, China. *Geology* 37, 515-518, doi: 10.1130/G25462A.1

Yao, H., Beghein, C. & van der Hilst, R. D., 2008. Surface wave array tomography in SE Tibet from ambient seismic noise and two-station analysis – II. Crustal and upper-mantle structure. *Geophys. J. Int.* 173, 205-219, doi: 10.1111/j.1365-246X.2007.03696.x

Yi, G. X., Yao, H. J., Zhu, J. S. & van der Hilst, R. D., 2008. Rayleigh-wave phase velocity distribution in China continent and its adjacent regions. *Chinese Journal of Geophysics-Chinese edition* 51, 402-411.

Yin, A., 2000. Mode of Cenozoic east –west extension in Tibet suggesting a common origin

of rifts in Asia during the Indo-Asian collision. *J. Geophys. Res.* 105, 21745–21759.

Yuan, X., Ni, J., Kind, R., Mechie, J. & Sandvol, E., 1997. Lithospheric and upper mantle structure of southern Tibet from a seismological passive source experiment. J. Geophys. Res. 102, 27491-27500.

Yuan, X., Kind, R. & Sobolev, S. V., 2002. Moho topography in the central Andes and its geodynamic implications. *Earth Planet. Sci. Lett.* 199, 389-402, doi:10.1016/S0012-821X(02)00589-7

Yusa, H. & Inoue, T., 1997. Compressibility of hydrous wadsleyite (β-phase) Mg_2SiO_4 by high pressure X-ray diffraction. *Geophys. Res. Lett.* 24, 1832-1834.

Zhang, P.Z., Xu, X.W., Wen X.Z., 2008. Slip rates and recurrence intervals of the Longmenshan active fault zone, and tectonic implications for the mechanism of the May 12 Wenchuan earthquake, 2008, Sichuan, *Chinese Journal of Geophysics-Chinese edition*, 51(4), 1066-1073.

Zhang, Z. J., Wang, Y. H., Chen, Y., Tian, X. B., Houseman, G., Wang, E. & Teng, J. W., 2009. Crustal structure across Longmenshan fault belt from passive source seismic profiling. *Geophys. Res. Lett*. 36, L17310, doi:10.1029/2009GL039580

Zhang Z.J., Klemperer S., 2010. Crustal structure of the Tethyan Himalaya, southern Tibet: new constrains from old wide-angle seismic data. *Geophysical Journal International*, in revision.

Zhu, L. P. & Helmberger, L. V., 1998. Moho offset across the northern margin of the Tibetan Plateau. *Science* 281, 1170-1172.

Table and Figure captions

Table 1: Depths of the LAB, and the 410 km and 660 km discontinuities beneath the 29 stations along the profile.

Figure 1: Topographic map of the eastern margin of the Tibetan plateau. The triangles denote seismic stations. The star is the epicenter of the Wenchuan earthquake (Ms = 8.0). Yellow circles mark the locations of the 461 aftershocks having Ms > 4.0 that occurred along the Longmen-Shan (LMS) fault. Inset is a map of the Tibetan plateau and its surrounding area. Arrows indicate GPS vectors after Gan et al. (2007).

Figure 2: (a) Distribution map of the events with Ms>5.0 and epicentral distances of 30-90° used in this study. **(b)** Raw P receiver functions for all 29 stations along the profile, grouped by stations and plotted at equal-spacing. Red and blue colors are used to shade the positive and negative amplitudes, respectively. The later part (>35 s) is lowpass filtered to 5 s. Main discontinuities are marked by Moho, LAB, 410-km and 660-km, respectively.

Figure 3: Migrated P receiver function image along the profile. P-to-S conversions from the Moho, the lithosphere-asthenosphere boundary (LAB) and the discontinuities around the 410 km and 660 km depth are clearly seen. Reddish colors indicate positive (velocity increasing downwards) and bluish negative (velocity decreasing downwards) signals.

Figure 4: (a) SP conversion point distribution at 100 km depth. Good S receiver functions have only been obtained from the Fiji-Tonga region. (**b)** S receiver function stacks in boxes defined in Figure 4a along the profile. The signal from the LAB is visible and marked by red dashed line. Blue dashed line marks the LAB from P receiver functions in Figure 3. The LAB

arrives in boxes 1-4 after about 9 s and in boxes 5-7 after about 12.5 s. Reference slowness for S receiver functions is 6.4 s/°, the same as for the P receiver functions , which makes P and S differential times directly comparable.

Figure 5: Binning stacks of P receiver functions along the seismic profile in Figure 1. The bins are defined using piercing points of P-to-S conversions at a depth of 530 km with a stacking width of 150 km and a moving step of 50 km. The red dashed lines indicate the arrivals of the P-to-S conversions predicted by the IASP91 model, the blue solid lines approximately mark the observed arrivals.

Figure 6: (a) Piercing points of P receiver functions at 410 and 660 km depths. They are grouped into two subsets to build two transects (AA'and BB'); **(b)** Migrated MTZ images along two transects (AA'and BB'). **(c)** Section of all receiver functions. The deepening of the 410 below eastern Tibet is visible especially in the AA'transect.

Figure 7: (a) Location map of permanent seismic broadband stations in China. The observed differential times of the 410 km and 660 km discontinuities corrected to a 67° epicentral distance are also shown. The IASP91 value is 24 s. No significant contiguous zone of a thickened MTZ related to the slab stagnation of the western Pacific subduction zone exists. The seismic profile from the Sichuan Basin is marked on the map. **(b)** Waveforms of the P-to-S conversions from the 410 km and 660 km discontinuities at the stations shown in (a) lined up along the 410 signal and sorted by increasing differential time. The maximum deviation from the 24 s global average value (marked by the blue line) is ±2 s, corresponding to a MTZ thickness variation of less than ±10%.

Figure 1

Click here to download Figure: Figure_1.pdf

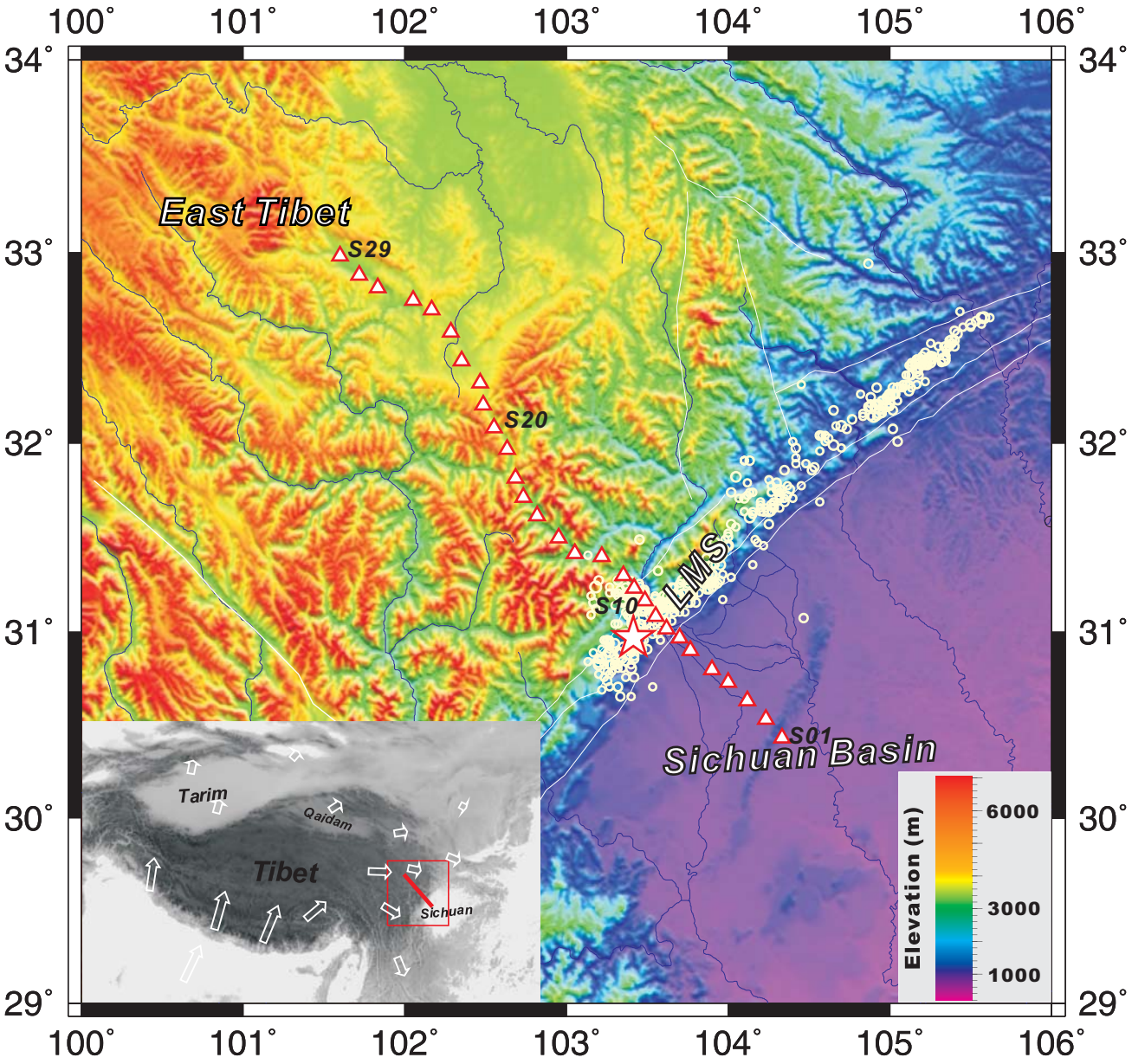

Figure 2a

Click here to download Figure: Figure_2a.pdf

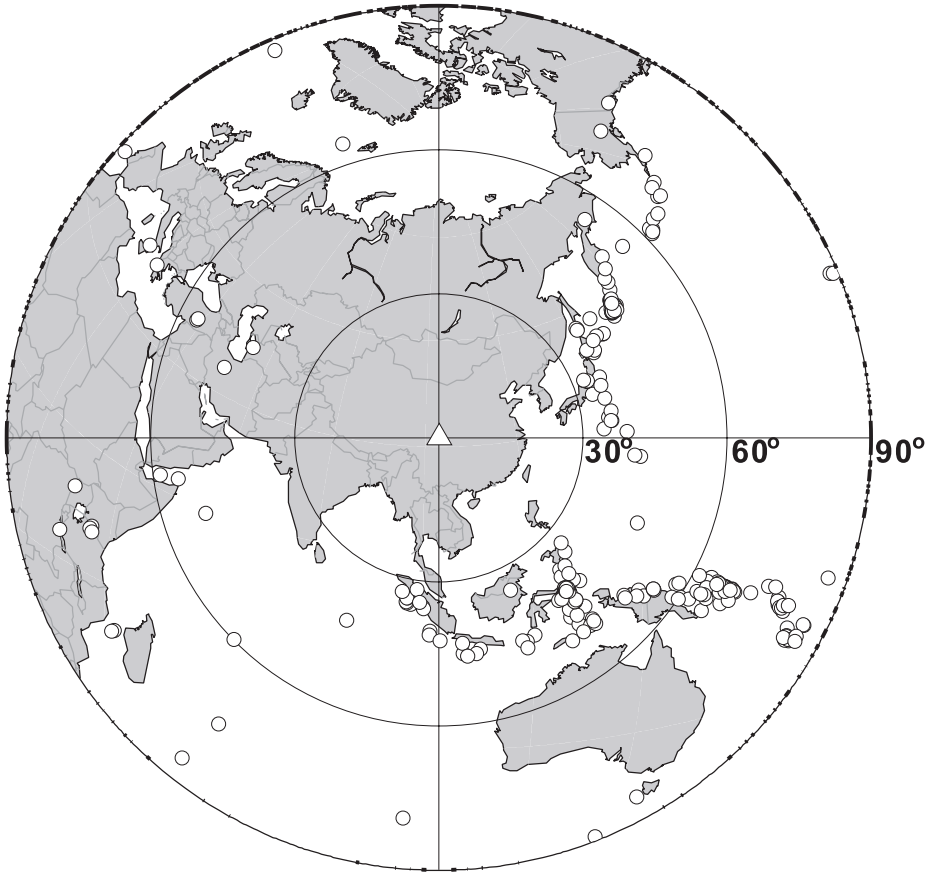

Figure 2b
Click here to download Figure: fig02_b.pdf

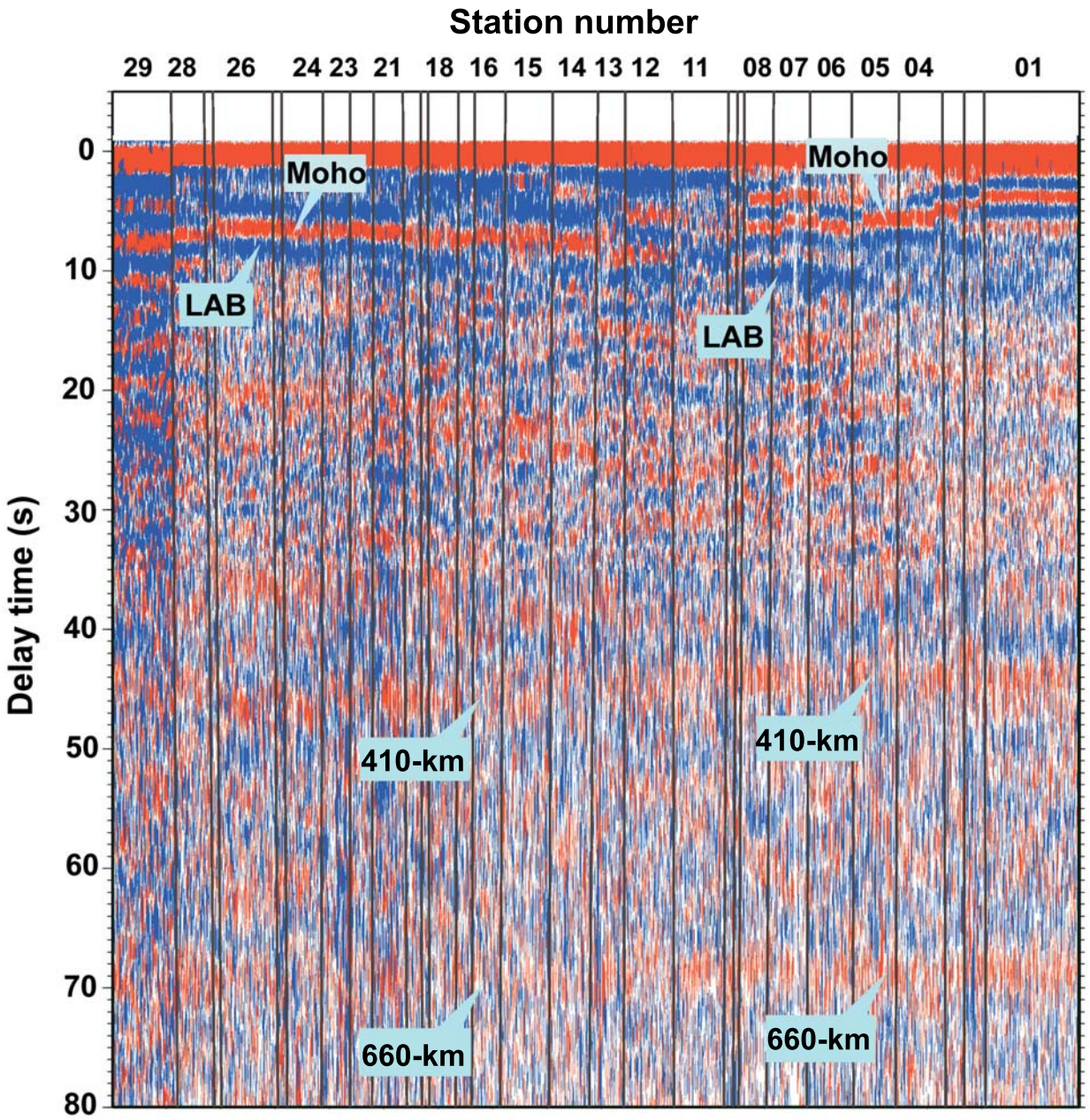

Figure 3

Click here to download Figure: Figure_3.pdf

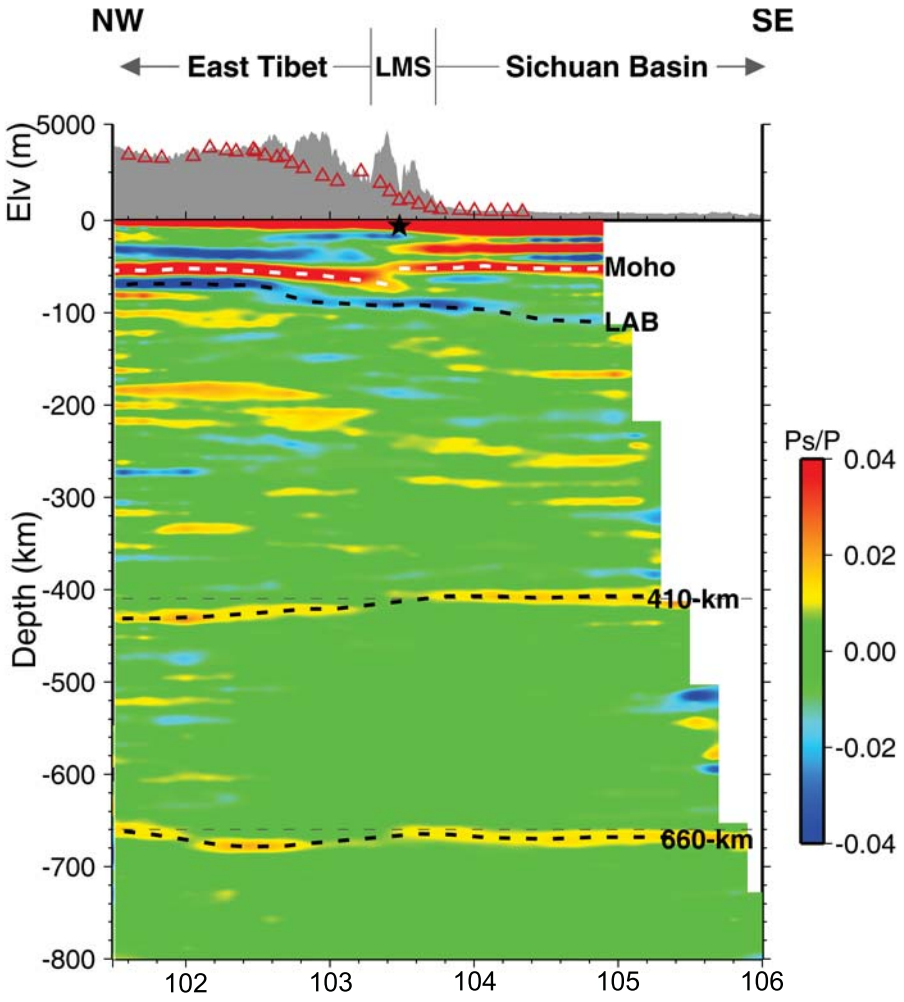

Figure 4

Click here to download Figure: Figure_4.pdf

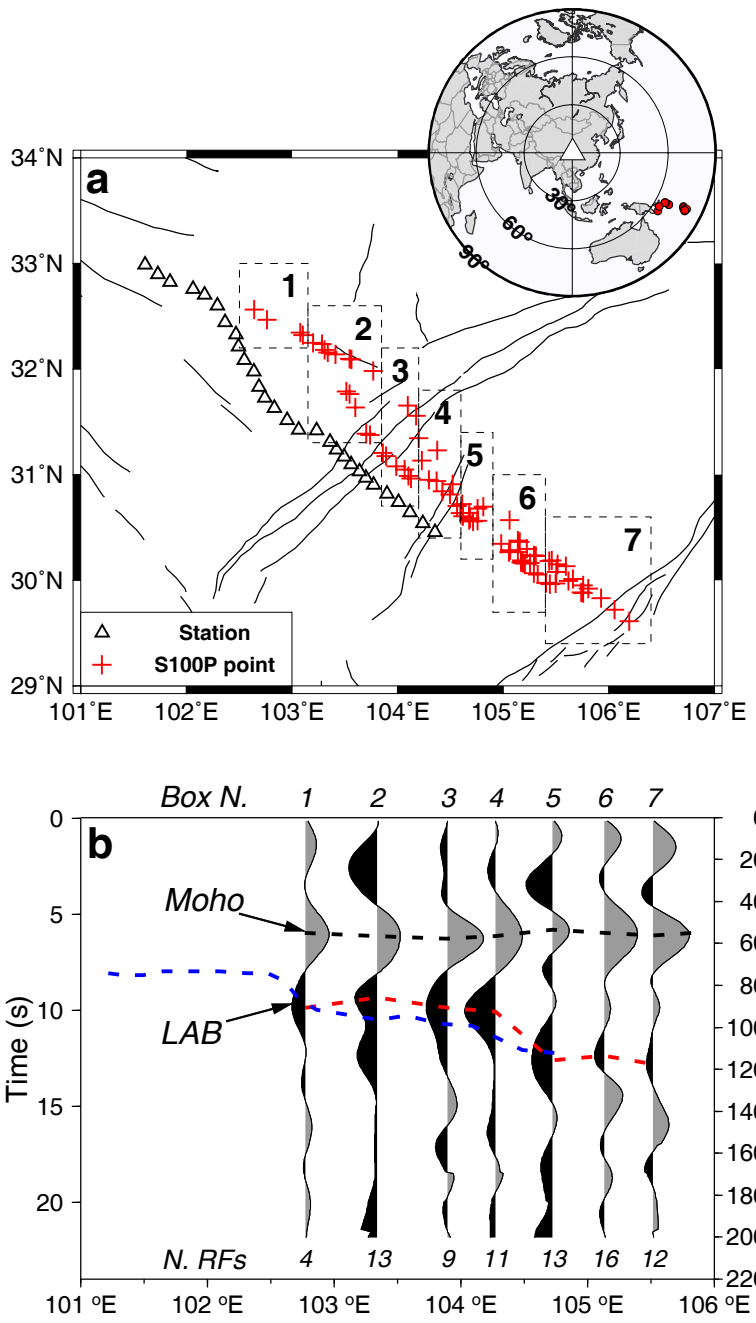

Figure 5

Click here to download Figure: Figure_5.pdf

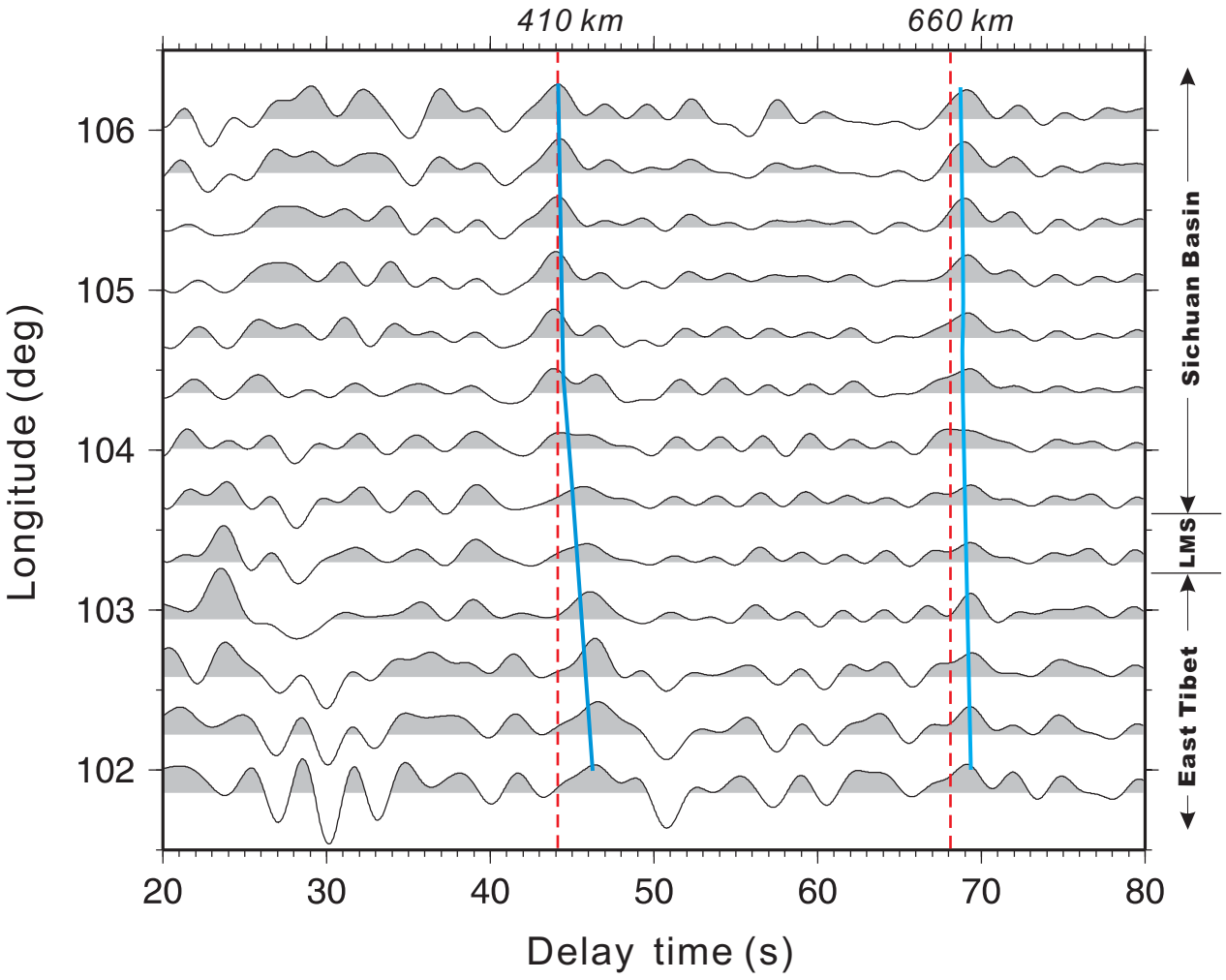

Figure 6

Click here to download Figure: fig06.pdf

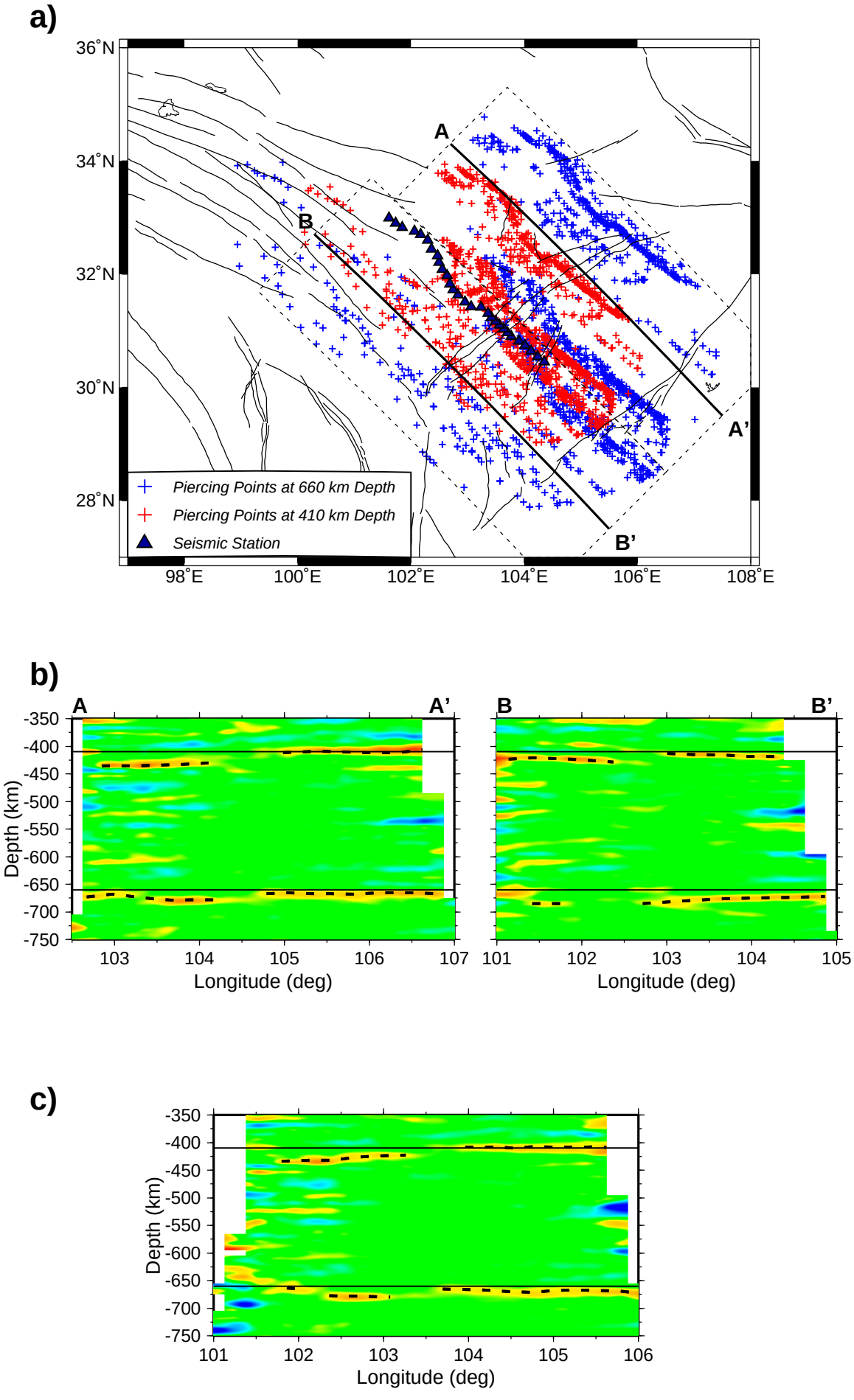

Figure 7a,b

Click here to download Figure: Figure 7a_b.doc

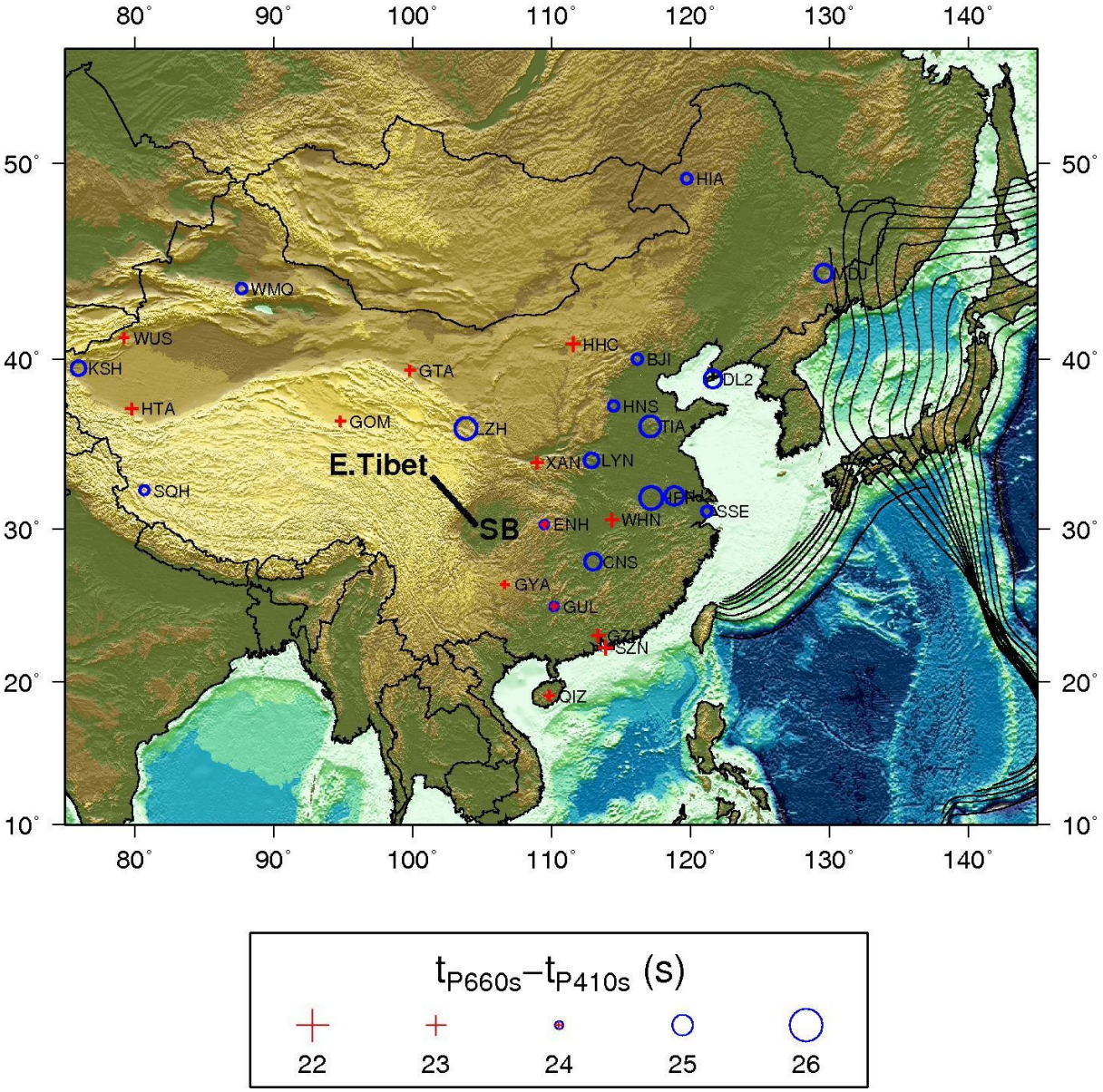

Figure 7a

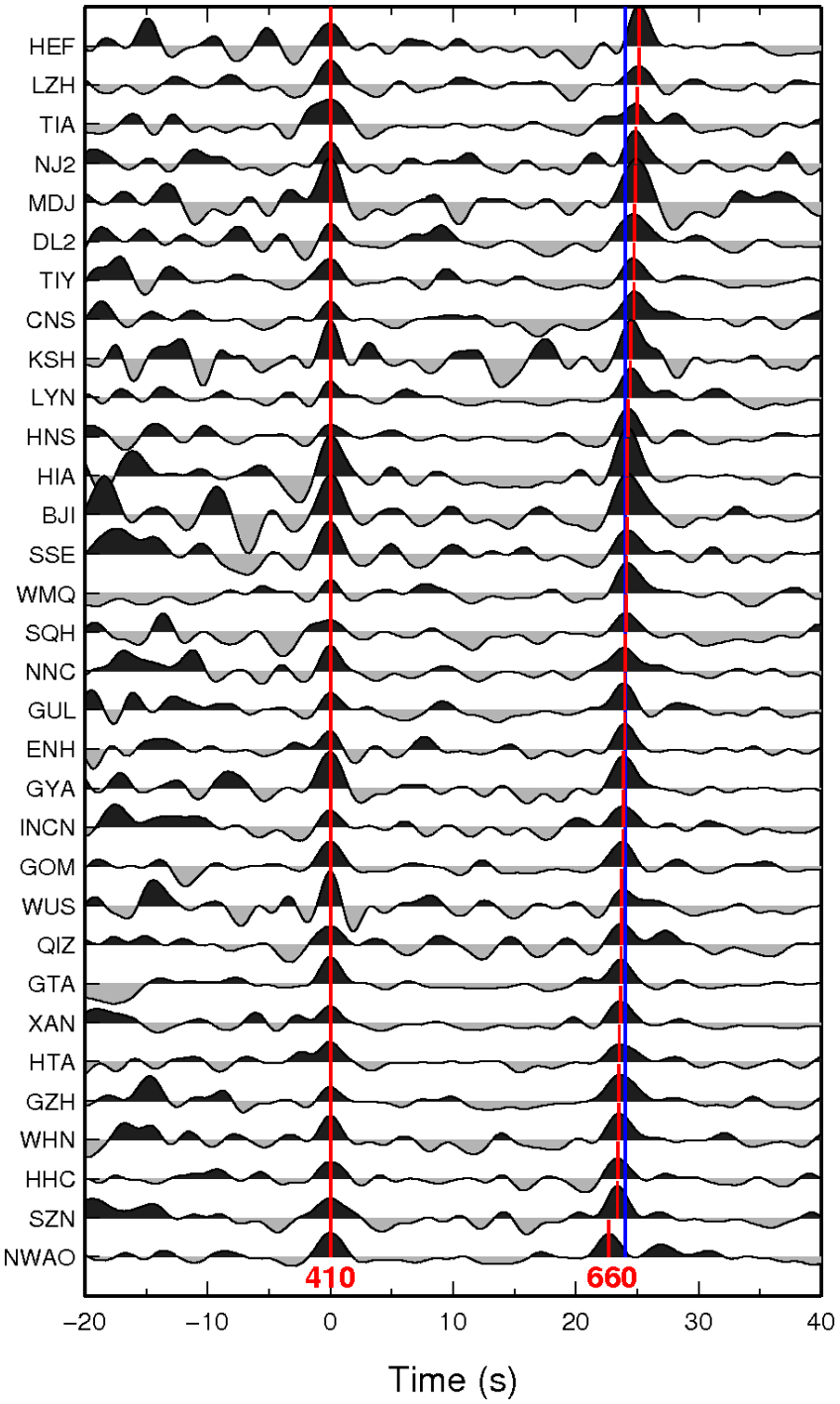
HEF
LZH
TIA
NJ2
MDJ
DL2
TIY
CNS
KSH
LYN
HNS
HIA
BJI
SSE
WMQ
SQH
NNC
GUL
ENH
GYA
INCN
GOM
WUS
QIZ
GTA
XAN
HTA
GZH
WHN
HHC
SZN
NWAO
410
660
−20
−10
0
10
20
30
40
Time (s)

Figure 7b

Table

Click here to download Table: Table_LAB_410_660.pdf

Station	Longitude (°)	Latitude (°)	LAB (km)	D410 (km)	D660 (km)
ST01	104.33	30.43	103	409	670
ST02	104.23	30.53	100	408	670
ST03	104.12	30.63	97	407	669
ST04	104	30.73	96	406	668
ST05	103.9	30.8	95	406	666
ST06	103.77	30.9	93	407	665
ST07	103.7	30.97	92	408	664
ST08	103.62	31.02	91	410	664
ST09	103.55	31.08	91	412	665
ST10	103.48	31.17	91	413	665
ST11	103.42	31.23	92	415	665
ST12	103.35	31.3	93	416	666
ST13	103.22	31.4	92	419	668
ST14	103.05	31.42	90	421	671
ST15	102.95	31.5	89	421	673
ST16	102.82	31.62	87	421	675
ST17	102.73	31.72	84	422	677
ST18	102.68	31.82	80	423	678
ST19	102.63	31.97	76	423	678
ST20	102.55	32.08	71	425	679
ST21	102.48	32.2	70	426	679
ST22	102.47	32.32	70	426	679
ST23	102.35	32.43	70	427	678
ST24	102.28	32.58	70	428	677
ST25	102.17	32.7	69	429	675
ST26	102.05	32.75	69	430	673
ST27	101.83	32.82	69	431	667
ST28	101.72	32.88	69	431	664
ST29	101.6	32.98	70	431	662